

# Numerical studies on the self-similar collapse of the $\alpha$ -patches problem

Ana M. Mancho

Instituto de Ciencias Matemáticas, CSIC-UAM-UC3M-UCM  
Serrano 121, Madrid 28006, Spain.

## Abstract

In this paper we study a class of contour dynamics equations depending on a parameter  $\alpha$  for which has been provided numerical evidence of self-similar collapse [2]. This family of equations connect the vortex patch problem of the 2D Euler equations (limit  $\alpha \rightarrow 0$ ) with the surface quasi-geostrophic equation ( $\alpha = 1$ ). We explore numerically the evolution of these equations, but in order to transform the finite time blowup in an asymptotic behaviour, the equations are expressed in self-similar variables. We discuss the role of exact self-similar solutions that act as geometrical separatrices of what numerically is distinguished as collapsing and non collapsing initial conditions.

Mathematics Subject Classification: 65M99, 35Q35

## 1 Introduction

A classical open problem in mathematical fluid mechanics is whether 3D Euler equations may develop singularities in finite time [1]. One of the scenarios proposed in the past for the formation of singularities in Euler equations is the vortex patch problem. A vortex patch consist of a 2D simply connected and bounded region of constant vorticity which is a weak solution of the 2D Euler equation. The work of Chemin [5] and Bertozzi and Constantin [3] rigorously proved global existence of regular solutions for this case, and therefore in the context of this equation, singularities cannot appear. A family of contour dynamics equations connect this scenario to the evolution of patches in the surface quasi-geostrophic equation. This problem, the  $\alpha$ -patches problem, has been analysed in [2] by Córdoba *et al.* It is described by the equation,

$$\frac{d\vec{x}(t)}{dt} = \sum_{k=1}^P \frac{\theta_k}{2\pi} \int_{C_k(t)} \frac{d\vec{x}_k}{|\vec{x}(t) - \vec{x}_k(t)|^\alpha}, \quad \vec{x} \in \mathbb{R}^2. \quad (1)$$

Here the sum extends up to  $P$ , the number of patches. This is a family of equations depending on the parameter  $\alpha$ . In the limit  $\alpha \rightarrow 0$  the equation

approach the vortex patch problem of the 2D Euler equation and the limit  $\alpha \rightarrow 1$  approaches the surface quasi-geostrophic equation. The later limit has been studied mathematically for more than a decade mainly because of its similarity to the 3D Euler equations [6] and because being a 2D model it is more tractable than the full 3D Euler system.

The solutions of the  $\alpha$ -patches problem have been numerically explored in the range  $0.5 \leq \alpha \leq 1$  (see the work by Córdoba *et al.* [2]) and it has been reported evidence of self-similar collapse. In this article we provide a detailed description of the numerical method used there to perform those simulations and also explain how it is applied to the study of the system expressed in self-similar variables. The advantage of using rescaled variables is that the finite time collapse observed by Córdoba *et al.*, becomes an asymptotic limit in the pseudo-time  $\tau$ , and thus the kind of evolution may be more accurately described. We have found a family of exact self-similar solutions to the rescaled system. Numerically is found that these solutions act as geometrical separatrices of collapsing and non collapsing initial conditions. This article describes these findings as follows. Section 2 describes the problem. In particular the equations under study are introduced and the derivation of the self-similar equations is explained. Section 3 reports on the numerical methods employed in the simulations. Section 4 accounts on the results. Finally section 5 presents the conclusions.

## 2 The equations

For the 2D vortex patch problem, the velocity of a particle on the contour of the patch is obtained, following Zabusky et al. [14], by inverting the relation between the streamfunction and the vorticity. For the  $\alpha$ -patches problem this relation is generalised by  $\theta = (-\Delta)^{1-\frac{\alpha}{2}}\psi$ , where  $\theta$  is the scalar and  $\psi$  is the streamfunction. In the limit  $\alpha \rightarrow 0$ , which corresponds to the 2D Euler equation, the scalar plays the role of vorticity and in the limit  $\alpha \rightarrow 1$  (the quasi-geostrophic equation) the scalar corresponds to the potential temperature. For  $0 < \alpha < 1$  one gets:

$$u(\vec{x}(\gamma, t), t) = \frac{\theta_1}{2\pi} \int_{C(t)} \frac{\frac{\partial \vec{x}}{\partial \gamma'}(\gamma', t)}{|\vec{x}(\gamma, t) - \vec{x}(\gamma', t)|^\alpha} d\gamma' \quad (2)$$

where  $\vec{x}(\gamma, t)$  is the position of points over the contour  $C(t)$ , parametrised with  $\gamma$ , and  $\theta_1 = \theta c_\alpha$ . Here  $\theta$  is the value of scalar in the patch and the factor  $c_\alpha = \frac{\Gamma(\frac{\alpha}{2})}{2^{1-\alpha}\Gamma(\frac{2-\alpha}{2})}$  results from inverting the operator  $(-\Delta)^{1-\frac{\alpha}{2}}$ . The contour dynamics equation is then obtained by stating:

$$\frac{d\vec{x}(\gamma, t)}{dt} = u(\vec{x}(\gamma, t), t) .$$

In this article we will focus on the contour evolution of two patches for which the equation become:

$$\frac{d\vec{x}(\gamma, t)}{dt} = \sum_{k=1}^2 \frac{\theta_k}{2\pi} \int_{C_k(t)} \frac{\frac{\partial \vec{x}_k}{\partial \gamma'}(\gamma', t) d\gamma'}{|\vec{x}(\gamma, t) - \vec{x}_k(\gamma', t)|^\alpha}, \quad (3)$$

Local existence for the limit  $\alpha = 1$  has been reported in [13, 18]. In this case one should use (see [13]) the following formula for the velocity (in the one patch case):

$$u(\vec{x}(\gamma, t), t) = \frac{\theta_1}{2\pi} \int_{C(t)} \frac{\frac{\partial \vec{x}}{\partial \gamma'}(\gamma', t) - \frac{\partial \vec{x}}{\partial \gamma}(\gamma, t)}{|\vec{x}(\gamma, t) - \vec{x}(\gamma', t)|^\alpha} d\gamma' \quad (4)$$

This equation eliminates the tangential component of the velocity, as only the normal component is able to deform the curve, and avoids therefore divergent integrals.

Simulations of Eq. (3) as reported in [2] show evidence of self-similar collapse. The singularity is point-like and we denote the collapse coordinates as  $\vec{x}_*(t_*)$ , where  $t_*$  is the collapse time. Numerical results of [2] indicate that near the blowup there exist scaling laws in the evolution of the maximum curvature as

$$\kappa \sim \frac{C}{(t_* - t)^{\frac{1}{\alpha}}} \quad \text{as } t \rightarrow t_*$$

and also in the minimum distance between contours

$$d \sim C(t_* - t)^{\frac{1}{\alpha}} \quad \text{as } t \rightarrow t_* \quad (5)$$

We re-scale the spatial variable as

$$\vec{x}(\gamma, t) - \vec{x}_*(t) = (t_* - t)^\delta (\vec{y}(\gamma, t) - \vec{y}_*), \quad (6)$$

where  $\delta = 1/\alpha$ , and the velocity of the scaling function  $\vec{x}_*(t)$  is given by

$$\frac{d\vec{x}_*(t)}{dt} = \sum_k \frac{\theta_k}{2\pi} \int_{C_k(t)} \frac{\frac{\partial \vec{x}_k}{\partial \gamma'}(\gamma', t) d\gamma'}{|\vec{x}_*(t) - \vec{x}_k(\gamma', t)|^\alpha}.$$

The equation of motion for the rescaled space variable  $\vec{y}$  is:

$$\begin{aligned} (t_* - t) \frac{\partial \vec{y}}{\partial t} - \delta(\vec{y} - \vec{y}_*) = \\ \sum_k \frac{\theta_k}{2\pi} \int_{\Upsilon_k(t)} \left( \frac{\frac{\partial \vec{y}_k}{\partial \gamma'}(\gamma', t)}{|\vec{y}(\gamma, t) - \vec{y}_k(\gamma', t)|^\alpha} - \frac{\frac{\partial \vec{y}_k}{\partial \gamma'}(\gamma', t)}{|\vec{y}_* - \vec{y}_k(\gamma', t)|^\alpha} \right) d\gamma' \end{aligned} \quad (7)$$

Where  $\Upsilon_k$  are the rescaled contours. The new time variable

$$\tau = -\log(t_* - t), \quad (8)$$

transforms the equation (7) into the self-similar equation:

$$\sum_k \frac{\theta_k}{2\pi} \int_{\Upsilon_k(\tau)} \left( \frac{\frac{\partial \vec{y}_k}{\partial \gamma'}(\gamma', \tau)}{|\vec{y}(\gamma, \tau) - \vec{y}_k(\gamma', \tau)|^\alpha} - \frac{\frac{\partial \vec{y}_k}{\partial \gamma'}(\gamma', \tau)}{|\vec{y}_* - \vec{y}_k(\gamma', \tau)|^\alpha} \right) d\gamma' \quad (9)$$

This equation, as the non-rescaled one, admits a projection over  $\vec{u}_n$ , the unitary normal component to the curve at  $\vec{y}$ , which is useful to describe the  $\alpha = 1$  case,

$$\frac{\partial \vec{y}}{\partial \tau} \cdot \vec{u}_n = (\delta(\vec{y} - \vec{y}_*)) \cdot \vec{u}_n + \left( \sum_k \frac{\theta_k}{2\pi} \int_{\Upsilon_k(\tau)} \left( \frac{\frac{\partial \vec{y}_k}{\partial \gamma'}(\gamma', \tau)}{|\vec{y}(\gamma, \tau) - \vec{y}_k(\gamma', \tau)|^\alpha} - \frac{\frac{\partial \vec{y}_k}{\partial \gamma'}(\gamma', \tau)}{|\vec{y}_* - \vec{y}_k(\gamma', \tau)|^\alpha} \right) d\gamma' \right) \cdot \vec{u}_n \quad (10)$$

The projection evolves in time the same as the system (9) as only the normal component deforms the curve. Near the collapse time, rescaled contours reported in the work by Córdoba et al. (see [2]) seem to coincide over a unique curve, thus suggesting that Eq. (10) has a fixed point, also called self-similar solution.

There exist interesting relations between the original and rescaled variables. For instance, the blowup in the original variables is transformed into an asymptotic behaviour in the self-similar variables. In this way the collapse reported in [2] that takes place in a very small time interval in original variables, is mapped to an infinite interval in rescaled variables, thus permitting a detailed monitoring of the blowup. We consider now the area of the patches. It is related to the energy of the initial data and it is conserved in the original variables  $(\vec{x}, t)$ , however following Eq. (6), it tends to grow in the rescaled  $(\vec{y}, \tau)$ . Other connections between the rescaled and non rescaled variables regard to distance. The shortest distance  $d$ , between collapsing contours (see Eq. (5)) tends to zero in the original variables but it is not necessarily zero in the new variables. In fact in [2] it is reported how the rescaled curves seem to keep a finite distance between them. These results are easily justified. Since collapse is point-like, at the blowup time distance between contours becomes zero just for two trajectories, one on each contour, satisfying,

$$|\vec{x}_{C_1}(t) - \vec{x}_{C_2}(t)| \rightarrow 0, \quad t \rightarrow t_* \quad (11)$$

Distance between these trajectories in self-similar variables, is given by,

$$|\vec{x}_{C_1}(t) - \vec{x}_{C_2}(t)| = (t_* - t)^\delta |\vec{y}_{C_1}(t) - \vec{y}_{C_2}(t)| \quad (12)$$

The factor  $(t_* - t)^\delta$  in Eq. (12) confirms that the null distance between the original variables is satisfied even if trajectories on the rescaled variables are at a finite distance at the collapse time  $t_*$ . The above expression may be rewritten in terms of the pseudo-time  $\tau$  as follows,

$$|\vec{x}_{C_1}(t) - \vec{x}_{C_2}(t)| = e^{-\tau\delta} |\vec{y}_{C_1}(\tau) - \vec{y}_{C_2}(\tau)| \quad (13)$$

As explained in next section, the numerical technique used for simulations does not track individual particles on contours, but just the contour as a whole, so that the above collapse trajectories are not numerically integrated. However it is expected that near the collapse, the distance between these trajectories will be well represented by the evolution of the shortest distance between contours for which in [2] it is reported

$$|\vec{x}_{c_1}(t) - \vec{x}_{c_2}(t)| \sim D \cdot (t_* - t)^{1/\alpha}, \quad t \rightarrow t_* \quad (14)$$

Here  $\vec{x}_{c_i}(t)$ ,  $i = 1, 2$  represents the set of points on the contours that are at a shortest distance, as a function of time. Similarly in the self-similar variables the collapse may be tracked by means of the shortest distance between contours,

$$|\vec{x}_{c_1} - \vec{x}_{c_2}| \sim e^{-\tau\delta} |\vec{y}_{c_1} - \vec{y}_{c_2}|, \quad (15)$$

This expression indicates that existence of collapse in the self-similar variables, implies that the minimum distance between contours defined as:

$$|\vec{y}_{c_1} - \vec{y}_{c_2}| \equiv D(\tau), \quad (16)$$

is a positive function,  $D(\tau)$ , satisfying:

$$\lim_{\tau \rightarrow \infty} \frac{D(\tau)}{e^{\tau\delta}} \rightarrow 0, \quad (17)$$

Otherwise the initial patches would be non collapsing. In other words, non collapsing patches, in the original variables remain always with finite curvature and at a finite distance at any time, but in the self-similar variables its minimum distance asymptotically goes at least as  $e^{\tau\delta}$ , so that they are repelled one from other. Typically the time evolution of non collapsing initial data is not described in the self-similar variables framework, however this is done in this article guided by the exact self-similar solutions of the system (9), for which numerics shows evidence that they constitute a boundary between collapsing and non collapsing data. We will come to these issues in detail in the results section. The existence of a  $\tau$  dependent function  $D(\tau)$ , is consistent with the collapse classifications in terms of self-similar variables reported in [15]. There it is shown that the asymptotic behaviour of the collapsing data may be towards a fixed point (a constant  $D(\tau)$ ) or towards  $\tau$ -dependent solutions which may be either periodic or chaotic. In this article we will show that numerical simulations indicate that the collapse of the  $\alpha$ -patches problem address an asymptotic chaotic regime, suggesting that this could be the type of collapse present in the 3D Euler problem as conjectured in [16].

### 3 The numerical method

We have numerically solved Eq. (3) for  $0 < \alpha < 1$ . The evolution is calculated using ideas developed in [8, 9] for the case of the 2D Euler equations. In

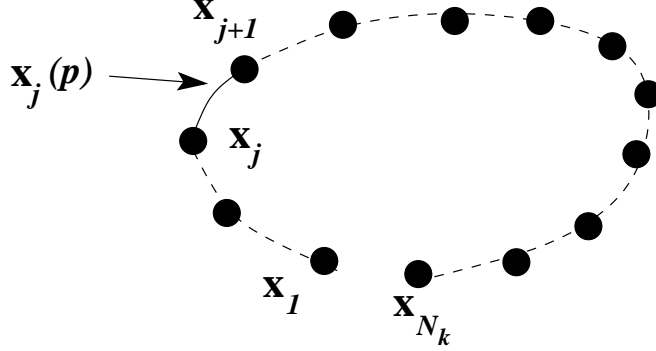


Figure 1: A representation of the contour  $C_k$  by a set of  $N_k$  points. The solid line represents the interpolating curve between nodes  $\vec{x}_j$  and  $\vec{x}_{j+1}$ .

particular, as described in [9], each contour  $C_k$  is represented by a set of nodes  $N_k$ . Fig. 1 depicts a scheme showing how the curve is interpolated between consecutive nodes with a cubic spline, as follows:

$$\vec{x}_j(p) = \vec{x}_j + p \vec{t}_j + \eta_j(p) \vec{n}_j \quad (18)$$

for  $0 \leq p \leq 1$  with  $\vec{x}_j(0) = \vec{x}_j$  and  $\vec{x}_j(1) = \vec{x}_{j+1}$ , where:

$$\vec{t}_j = (a_j, b_j) = \vec{x}_{j+1} - \vec{x}_j, \quad \vec{t}_j \in \mathbb{R}^2 \quad (19)$$

$$\vec{n}_j = (-b_j, a_j), \quad \vec{n}_j \in \mathbb{R}^2 \quad (20)$$

$$\eta_j(p) = \mu_j p + \beta_j p^2 + \gamma_j p^3, \quad \eta_j \in \mathbb{R}. \quad (21)$$

The cubic interpolation coefficients  $\mu_j$ ,  $\beta_j$  and  $\gamma_j$  are:

$$\mu_j = -\frac{1}{3}d_j\kappa_j - \frac{1}{6}d_j\kappa_{j+1}, \quad \beta_j = 2d_j\kappa_j, \quad \gamma_j = \frac{1}{6}d_j(\kappa_{j+1} - \kappa_j),$$

where  $d_j = |\vec{x}_{j+1} - \vec{x}_j|$  and

$$\kappa_j = 2 \frac{a_{j-1}b_j - b_{j-1}a_j}{|d_{j-1}^2 \vec{t}_j + d_j^2 \vec{t}_j - 1|} \quad (22)$$

is the local curvature defined by a circle through the three points,  $x_{j-1}$ ,  $x_j$ , and  $x_{j+1}$ . The node spacing in each contour is non-locally adjusted at each time step depending on curvature. Issues related to the density of nodes along the curve will be addressed later. Now it is explained how the system (3) is transformed by the above discretisation. The evolution of any point  $\vec{x}(\gamma, t)$  on the contours is replaced by the evolution of a point  $\vec{x}_j$  on the discrete curves, and the integrals on the contour curves  $C_k$  are replaced by the summation of integrals over the parameter  $p$ :

$$\frac{d\vec{x}_j(t)}{dt} = \sum_{k=1}^2 \frac{\theta_k}{2\pi} \sum_{i=1}^{N_k} \int_0^1 \frac{\frac{\partial \vec{x}_{i,k}(p,t)}{\partial p} dp}{|\vec{x}_j(t) - \vec{x}_{i,k}(p,t)|^\alpha}, \quad (23)$$

here  $\vec{x}_{i,k}(p, t)$  refers to a piece of curve computed as in Eq. (18) at a time  $t$ , and the additional subindex  $k$  distinguishes the contour where the segment is placed. More abstractly this expression may be written as:

$$\frac{d\vec{x}_j(t)}{dt} = f_j(\vec{x}_j(t), C_1, C_2), \quad f_j : \mathbb{R}^2 \rightarrow \mathbb{R}^2 \quad (24)$$

This equation stands for any node  $\vec{x}_j$  on the discretised contour curves so, for the case of two contours on a plane, the system (23) represents a set of  $M = 2 \times (N_1 + N_2)$  coupled ordinary differential equations, which more compactly is rewritten as an autonomous system as follows:

$$\frac{d\mathbf{x}}{dt} = \mathbf{f}(\mathbf{x}), \quad \mathbf{x} \in \mathbb{R}^M \quad (25)$$

The dimension  $M$  of the system (25) is very large and typically non constant, as the discretisation does not force to maintain the number of points  $N_k$  on the curve for all times. Following [9] the system (25) is integrated with an explicit 4<sup>th</sup> order Runge-Kutta method. The time step  $\Delta t$  in the Runge-Kutta method as suggested by Córdoba et al. [2] is chosen dynamically, since near the collapse time it has to be refined. As it is reported there, the blowup concurs with the formation of corners on the contours, and the node spacing  $\Delta x$  is reduced to represent corners properly. The time step is then adjusted as  $\Delta t = B\Delta x$ , where  $B$  is empirically tuned for different values of  $\alpha$ .

In the numerical simulation of the  $\alpha$ -patches problem the most challenging part is the evaluation of each  $f_j$  in Eq. (24) as required by the Runge-Kutta method at each time step. In order to explain how this is achieved, next focus is on the contour integrals along each cubic contour segment (see Eq. (23)). In this equation the interpolation (18) is replaced and integrals are leaved as follows:

$$\begin{aligned} & \int_0^1 \frac{((\vec{t}_i + \mu_i \vec{n}_i) + (2\beta_i p + 3\gamma_i p^2) \vec{n}_i) dp}{|\vec{x}_i - \vec{x}_j + p \vec{t}_i + \eta_i(p) \vec{n}_i|^\alpha} = \\ & (\vec{t}_i + \mu_i \vec{n}_i) \int_0^1 \frac{dp}{|\vec{x}_i - \vec{x}_j + p \vec{t}_i + \eta_i(p) \vec{n}_i|^\alpha} + \vec{n}_i \int_0^1 \frac{(2\beta_i p + 3\gamma_i p^2) dp}{|\vec{x}_i - \vec{x}_j + p \vec{t}_i + \eta_i(p) \vec{n}_i|^\alpha}, \end{aligned} \quad (26)$$

The subindexes  $k$  appearing in integrals of Eq. (23) have been dropped to avoid cumbersome notation without lost of generality. Attending to the relative position of the variable  $\vec{x}_j$  versus the fixed  $\vec{x}_i$  we classify the kind of integrals to do.

**1.** The case  $\vec{x}_j = \vec{x}_i$ . In this situation the first integral on the right hand side of Eq. (26) has an integrand that becomes infinity at  $p = 0$ . However in spite of this the principal value of the integral is defined if  $\alpha < 1$ . In order to

compute the PV we rewrite the integral as follows:

$$\begin{aligned}
& \int_0^1 \frac{dp}{|p \vec{t}_i + \eta_i(p) \vec{n}_i|^\alpha} = \\
& \frac{1}{|\vec{t}_i|^\alpha} \frac{1}{(1 + \mu_i^2)^{\alpha/2}} \int_0^1 \frac{p^{-\alpha} dp}{\left(1 + \frac{\beta_i^2 p^2 + \gamma_i^2 p^4 + 2\mu_i \beta_i p + 2\mu_i \gamma_i p^2 + 2\beta_i \gamma_i p^3}{(1 + \mu_i^2)}\right)^{\alpha/2}} \\
& = \frac{1}{|\vec{t}_i|^\alpha} \frac{1}{(1 + \mu_i^2)^{\alpha/2}} \int_0^1 p^{-\alpha} (c_0 + c_1 p + c_2 p^2) + \mathcal{O}(p^3) \\
& \sim \frac{1}{|\vec{t}_i|^\alpha} \frac{1}{(1 + \mu_i^2)^{\alpha/2}} \sum_{n=0}^{10} \frac{c_n}{n - \alpha + 1}, \quad (27)
\end{aligned}$$

Coefficients on the expansion may be easily computed with Maple or Mathematica or other algebraic manipulator. In our numerical computations we have used an expansion up to the tenth order, which is very accurate as coefficients  $c_n$  rapidly decay. We provide an explicit expression for  $c_0$  and  $c_1$ .

$$c_0 = 1, \quad c_1 = -\frac{\alpha \mu_i \beta_i}{1 + \mu_i^2}$$

These coefficients are also useful to approach the second integral on the right hand side of Eq. (26). In particular this integral is approached by the summation:

$$\frac{1}{|\vec{t}_i|^\alpha} \frac{1}{(1 + \mu_i^2)^{\alpha/2}} \sum_{n=0}^{10} c_n \left( \frac{2\beta_i}{n - \alpha + 2} + \frac{3\gamma_i}{n - \alpha + 3} \right), \quad (28)$$

**2.** The case  $\vec{x}_j = \vec{x}_{i+1}$ . In this situation the first integral on the right hand side of Eq. (26) has an integrand that becomes infinity at  $p = 1$ , as  $x_i(p = 1) = x_{i+1}$ . Results described in **1.** are applicable here if integrals are rewritten for  $p' = 1 - p$ ,  $\tilde{\mu}_i = \mu_i + 2\beta_i + 3\gamma_i$ ,  $\tilde{\beta}_i = -\beta_i - 3\gamma_i$  and  $\tilde{\gamma}_i = \gamma_i$ .

**3.** The case  $d_x = |\vec{x}_j - \vec{x}_i| > 0$ . In this case the first integral on the right hand side of Eq. (26) may be approached by a series expansion as follows:

$$\begin{aligned}
& \int_0^1 \frac{dp}{|\vec{x}_i - \vec{x}_j + p \vec{t}_i + \eta_i(p) \vec{n}_i|^\alpha} = \\
& \frac{1}{d_x^\alpha} \int_0^1 \frac{dp}{\left(1 + \frac{p^2 |\vec{t}_i|^2 + \eta_i(p)^2 |\vec{n}_i|^2 + d_t p + d_n \eta_i(p)}{d_x^2}\right)^{\alpha/2}} \sim \frac{1}{d_x^\alpha} \sum_{n=0}^{10} g_n \quad (29)
\end{aligned}$$

where  $d_n = -(\vec{x}_j - \vec{x}_i) \cdot \vec{n}$  and  $d_t = -(\vec{x}_j - \vec{x}_i) \cdot \vec{t}$ , and coefficients are computed with a software for algebraic manipulation. Coefficients  $g_n$  rapidly decay if the distance,  $d_x$ , between  $\vec{x}_j$  and  $\vec{x}_i$  is large enough. We provide an explicit expression for  $g_0$  and  $g_1$ :

$$g_0 = 1, \quad g_1 = -\frac{\alpha(d_t + d_n \mu_i)}{2d_x^2}, \dots$$



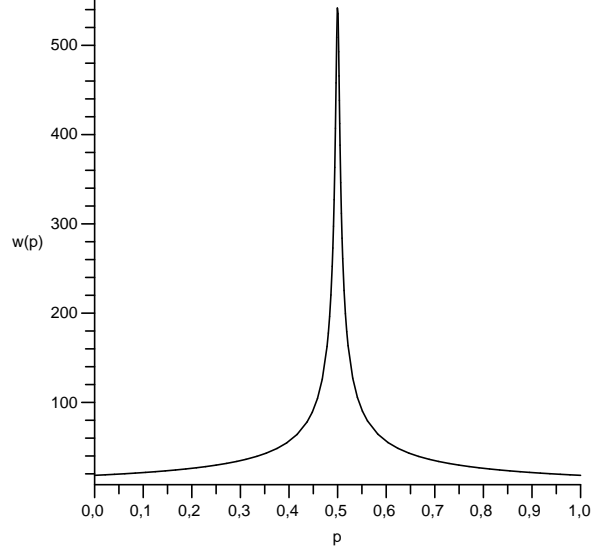


Figure 2: A graphic of the integrand in the first integral at the right hand side of Eq. (26) in the case  $|\vec{x}_j - \vec{x}_i| \sim 0$ . It may vary steeply in the domain.

The second integral on the right hand side of Eq. (26) may also be expressed in terms of coefficients  $g_n$ .

4. The case  $|\vec{x}_j - \vec{x}_i| \sim 0$ . In this situation the first integral at the right hand side of Eq. (26) has an integrand  $w(p)$  which for instance may take the appearance depicted in Fig. 2. As noted there, it may vary steeply in the domain. In this case we compute the area below the function:

$$\int_0^1 w(p) dp = A$$

by integrating the following ordinary differential equation:

$$\frac{dY}{dp} = w(p)$$

with initial condition  $Y(p = 0) = 0$ . With this choice the integrated function will be such that  $Y(p = 1) = A$ . The integration method used is a variable step 5<sup>th</sup> order Runge-Kutta method (see [17]), thus ensuring it will appropriately track steep variations. The evaluation of  $w(p)$  must be done with a lot of care to avoid round off errors. This is correctly done if the denominator in Eq. (26) is computed as follows. First the polynomial in  $p$  is expanded and the coefficient of each monomial in  $p$  is evaluated. Second these terms are added up.

In the numerical code an appropriate test distinguishes which one of these procedures needs to be followed to evaluate an integral. The code is verified by

evaluating  $f_j(\vec{x}_j, C_1)$  for a case with only one contour, the circle of radius 1 centred at the origin,  $\vec{x}_j = (1, 0)$  and  $\theta_1 = -1$ . The output of the discrete scheme just explained is compared with that obtained from the natural parametrisation in  $\theta$ , i.e.  $C_1 = (\cos(\theta), \sin(\theta))$ ,  $\theta \in [0, 2\pi]$ . In this case the integral to evaluate is:

$$f_j(\vec{x}_j, C_1) = \frac{-1}{2\pi} \int_0^{2\pi} \frac{(-\sin \theta, \cos \theta) d\theta}{\left(\sqrt{(1 - \cos \theta)^2 + \sin^2 \theta}\right)^\alpha}.$$

This integral is numerically evaluated with Maple forcing 5 digits precision, which gives  $f_j(\vec{x}_j, C_1) = (9.549296 \cdot 10^{-15}, -8.4000655 \cdot 10^{-1})$ . The above numerical method considering 200 points on the circle supplies:  $f_j(\vec{x}_j, C_1) = (-3.09849665 \cdot 10^{-5}, -8.39990851 \cdot 10^{-1})$ . Both results agree within reasonable accuracy. The precision of the numerical method depends on the number of points on the discretised curve, and also on certain tolerance in the criteria used to distinguish between the application of the procedure 3 or 4 discussed above. In practise evaluation of  $f_j$  is accurate up to the 5<sup>th</sup> digit in consistency with the 4<sup>th</sup> order Runge-Kutta method employed to evolve  $\mathbf{x}$ .

The evolution of the quasi-geostrophic equation (i.e the case  $\alpha = 1$ ) as reported in Eq. (4) is computed projecting the vector field of Eq. (3) over the unitary normal component to the curve at  $\vec{x}_j$ . This means that numerically the first integral at the right hand side of Eq. (26) needs not to be computed (in fact it is a divergent integral (see [13])) as it is a tangential component to the curve at  $\vec{x}_j$ . The second integral at the right hand side of Eq. (26) need to be projected over the unitary normal component to the curve, and this is easily done. The evolution of the contours for  $\alpha < 1$  may be indistinctly computed either with Eq. (3) or with Eq. (4).

Once  $\mathbf{f}(\mathbf{x})$  in Eq. (25) is conveniently approached we are ready to apply the 4<sup>th</sup> order Runge-Kutta method to step forward  $\mathbf{x}$ . Following the methodology developed in [9] every time step the nodes are redistributed on the contour to guarantee its optimal representation. This means that the numerical method will not track individual trajectories, but the whole contour. The relocation of points is done as follows. For each node assume a local density

$$\rho_i = \frac{\hat{\kappa}_i}{1 + \delta \hat{\kappa}_i / \sqrt{2}}$$

This form limits the minimum distance between nodes to nearly  $\delta$  and the maximum computed curvature to  $\delta^{-1}$ . We take  $\delta = 10^{-6}$ . Here  $\hat{\kappa}_i = (\tilde{\kappa}_i + \tilde{\kappa}_{i+1})/2$  and

$$\tilde{\kappa}_i = (\nu L)^{-1}(\check{\kappa}_i L)^a + \sqrt{2}\check{\kappa}_i$$

We have considered  $L = 3$ ,  $a = 2/3$ , and  $\nu$  is a parameter which controls the accuracy of the representation, being 0.05 or 0.03 typical values for  $\nu$ . Smaller values imply larger densities of points on the curve. The curvature  $\check{\kappa}$  incorpo-

rates non-local effects and is defined as:

$$\check{\kappa}_i = \sum_j \frac{d_j |\bar{\kappa}_j|}{h_{ij}^2} \left( \sum_j \frac{d_j}{h_{ij}^2} \right)^{-1}$$

where  $d_j = |\vec{x}_{j+1} - \vec{x}_j|$ ,  $h_{ij} = |\vec{x}_i - (\vec{x}_{j+1} + \vec{x}_j)/2|$  and  $\bar{\kappa}_j = (\kappa_j + \kappa_{j+1})/2$  (see  $\kappa_j$  defined in Eq. (22)) and the summation is over all nodes in the contour of the node  $i$ .

Given a desired density  $\rho_i$  between nodes  $i$  and  $i+1$ , it is possible to compute  $\sigma_i = \rho_i d_i$ , which is the fractional number of nodes to be placed between  $i$  and  $i+1$ . The node redistribution in a contour  $k$  fixes one point on the curve, the first point, which will be kept fixed on the redistribution procedure. This implies that this point will evolve as a real trajectory of the system (25). The quantity  $q$  is computed:

$$q = \sum_{i=1}^{N_k} \sigma_i$$

and  $\tilde{N}_k = [q] + 2$ , the nearest integer to  $q$  plus two. The  $N_k - 1$  'old' nodes on the curve, will be replaced by  $\tilde{N}_k - 1$  new nodes which will lie along the curved contour segments connecting the old nodes. Let  $\sigma'_i = \sigma_i \tilde{N}_k / q$ , so that  $\sum_{i=1}^{N_k} \sigma'_i = \tilde{N}_k$ . Then the positions of the new nodes  $j = 2 \dots \tilde{N}_k$  are found successively by seeking  $i$  and  $p$  such that:

$$\sum_{l=1}^{i-1} \sigma'_l + \sigma'_i p = j - 1 \quad (30)$$

and placing each new node  $j$  between the old nodes  $i$  and  $i+1$  at the position  $\vec{x}_i(p)$  given by Eq. (18).

The evolution of the self-similar equation (9) may also be computed numerically, as its discrete version may formally be rewritten as:

$$\frac{d\vec{y}_j(\tau)}{d\tau} = F_j(\vec{y}_j, \Upsilon_1, \Upsilon_2), \quad F_j : \mathbb{R}^2 \rightarrow \mathbb{R}^2 \quad (31)$$

The numerical evaluation of  $F_j$  at each step of the 4<sup>th</sup> order Runge-Kutta method may be easily achieved with the use of the algorithm developed for the function  $f_j$  as it is satisfied that:

$$F_j(\vec{y}_j, \Upsilon_1, \Upsilon_2) = \delta \vec{y}_j + f_j(\vec{y}_j, \Upsilon_1, \Upsilon_2) - f_j(\vec{0}, \Upsilon_1, \Upsilon_2)$$

where the choice  $\vec{y}_* = \vec{0}$  has been considered.

## 4 The results

The numerical scheme explained above has been applied in [2] to simulate the time evolution of two identical circular patches of unit radius with centres placed

at a distance 2.5 and such that  $\theta_k = -1$  for  $k = 1, 2$ . In particular Eq. (3) is studied for  $0.5 \leq \alpha < 1$  and Eq. (4) for the case  $\alpha = 1$ . In Ref. [2] it is provided evidence of the evolution of the initial data towards a collapse presenting a rather stationary rescaled profile. Simulations performed in [2] were not implemented in the self-similar variables, and as novelty the results discussed in this article adopt the perspective of the self-similar variables. This section discusses the exact and numerical solutions to Eq. (9). Exact results are valid in the range  $0 < \alpha \leq 1$ , which encompasses the quasi-geostrophic equation. Numerical simulations have been just obtained for  $\alpha = 0.7$ , although they are expected to reflect the evolution on a whole  $\alpha$ -range.

#### 4.1 The self-similar solution

There exist exact self-similar solutions for contours  $\Upsilon_1$  and  $\Upsilon_2$  in Eq. (10). As expected from rescaling (6) at the collapse time  $t_*$  the area within self-similar contours is infinite. Stationary-like profiles of the rescaled curves presented in [2] suggest that each of these curves take the form of a function  $\Upsilon = (x, y(x))$ . When curves are parametrised as functions Eq. (10) is rewritten as:

$$\begin{aligned} \frac{\partial \vec{y}}{\partial \tau} \vec{u}_n &= (\delta(\vec{y} - \vec{y}_*)) \vec{u}_n + \frac{\theta_0}{2\pi} \left( \int_{\mathbb{R}} \frac{\frac{\partial \vec{y}_1}{\partial x'}(x', \tau) dx'}{|\vec{y}(x, \tau) - \vec{y}_1(x', \tau)|^\alpha} - \int_{\mathbb{R}} \frac{\frac{\partial \vec{y}_2}{\partial x'}(x', \tau) dx'}{|\vec{y}(x, \tau) - \vec{y}_2(x', \tau)|^\alpha} - \right. \\ &\quad \left. \int_{\mathbb{R}} \frac{\frac{\partial \vec{y}_1}{\partial x'}(x, \tau) dx'}{|\vec{y}_* - \vec{y}_1(x', \tau)|^\alpha} + \int_{\mathbb{R}} \frac{\frac{\partial \vec{y}_2}{\partial x'}(x', \tau) dx'}{|\vec{y}_* - \vec{y}_2(x', \tau)|^\alpha} \right) \vec{u}_n \end{aligned} \quad (32)$$

A fixed point to Eq. (32) is:

$$\Upsilon_1 = (x, |x|), \quad \Upsilon_2 = (x, -|x|) \quad (33)$$

These curves touch each other at one point, what is compatible with results on regularity of the contours discussed in [18]. Figure 3 shows geometrically how over these particular curves, the contributions of different terms of Eq. (32) to a point, marked with a black dot, cancel each other out. The first term of Eq. (32) evaluated at the black dot, provides a null contribution on the normal direction, as the arrow labelled with '1', is tangent to the curves (33). Arrows labelled with '2' and '3' show the normal component of the small contributions of the second and third terms of Eq. (32) integrated along the small segments within the gray dots. They cancel each other as they are equal magnitude but opposite sign. Similarly contributions from the 4<sup>th</sup> and 5<sup>th</sup> terms cancel each other.

The fixed point in Eq. (33) is not unique, as any rotation of it around the origin is also a stationary solution of Eq. (10). There exist infinite stationary solutions, related each other by this continuous transformation. There exist previous examples in the context infinite dimensional dynamical systems, of families of fixed points related by means of a group action (see for instance

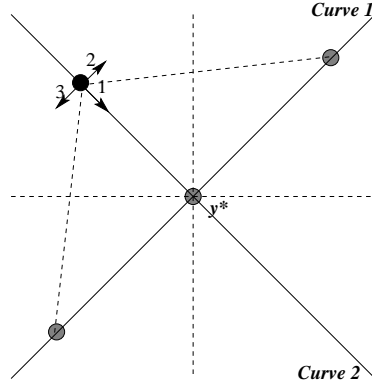


Figure 3: Sketch showing contributions of different terms in Eq. (32) to the point distinguished with a black dot. Each arrow is labelled with the number of the term it corresponds. It is clear that the geometry of the curves imposes cancellations of the normal components.

[20]). It has been reported [20] that this transformation implies the existence of a null eigenvalue along a dynamically neutral eigenspace. Apart from these fixed points, there might be other stationary solutions to Eq. (10), however we have not found those. Fixed points in the theory of dynamical system are particularly useful solutions, as they geometrically organise the flow on the phase space. Eq. (10) can be viewed as a dynamical system of infinite dimension that can be represented by a large number of equations as in Eq. (25). The fixed point in Eq. (33) is not a global attractor of (10). This could not be the case as otherwise every initial condition would be attracted by it, and this would imply non existence of non collapsing solutions. On the hand conservative systems, as is the case of the non rescaled system, do not have solutions which are attractors. Numerical simulations confirm the existence of perturbations to the curves (33) which are completely unstable. Figure 4a) shows the backwards time evolution of an initial condition which is a small perturbation to the self-similar functions (33). This initial data after 14 time steps with negative  $\Delta t$  approaches more and more the fixed point, implying that this perturbation is completely contained in the unstable subspace of (33). Figure 4b) displays the evaluation of the modulus of the normal component of the velocity along these curves and as expected it is almost zero. In these simulation curves  $\Upsilon_1$ ,  $\Upsilon_2$  have been transformed in functions with the asymptotic behaviour at large  $x$  extended with straight lines following the self-similar behaviour. These lines are large but not infinity, thus errors are introduced at their boundaries, however these errors are very small in the displayed zones.

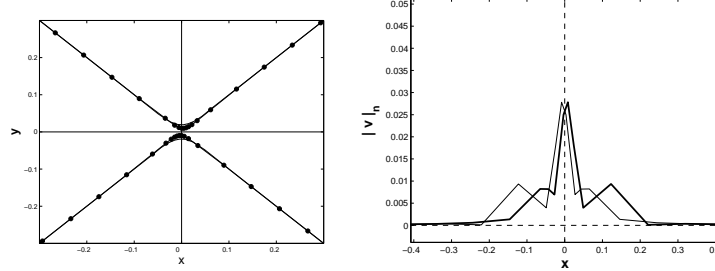


Figure 4: a) Initial data (solid line) and its backwards time evolution (line with circles) according to Eq. (10); b) Modulus of the normal component of the velocity along the initial data curves. Solid thick line corresponds to the lower curve, while thin line corresponds to the upper curve.

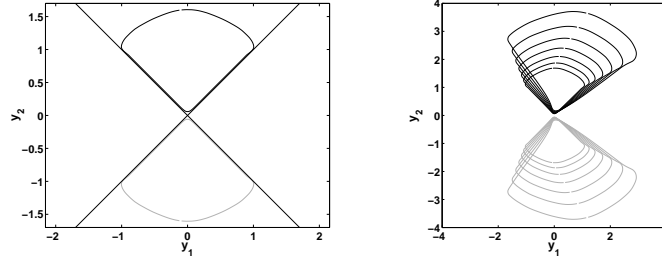


Figure 5: a) Initial data and the self-similar solution; b) Repelling  $\tau$  evolution of the patches in a).

## 4.2 The separatrix and the 'chaotic' collapse

The evolution of curves  $\Upsilon_1$ ,  $\Upsilon_2$  is described in self-similar variables. As it has been already pointed out, from Eq. (6) follows that in these coordinates the area enclosed by the contours becomes infinite at the collapse time  $t_*$ , but on the other hand blowup takes place at infinite time in the pseudo-time  $\tau$ , as transformation (8) confirms. This implies that at any stage of the simulation of Eq. (9),  $\tau$  and also the area of the patches are both finite, making possible the numerical computation of its evolution.

The solution (33) divides the plane in four domains that are labelled as the upper (U), the bottom (B), the right (R) and the left (L). The distribution of the patches over these regions provide configurations of collapse. In fact numerical evidence is found on the role of the fixed point (33) acting as a separatrix between non collapsing and collapsing initial data. In particular as discussed next a non collapse configuration of the initial data cannot cross the boundaries of the fixed point.

Figure 5a) displays two patches that initially stay very close each other, but at the same time they closely follow the fixed point (33) plus a small perturbation in the unstable subspace. This initial data is entirely contained in the upper (U) and lower (L) domains. Figure 5b) confirms the repelling  $\tau$  evolution of this

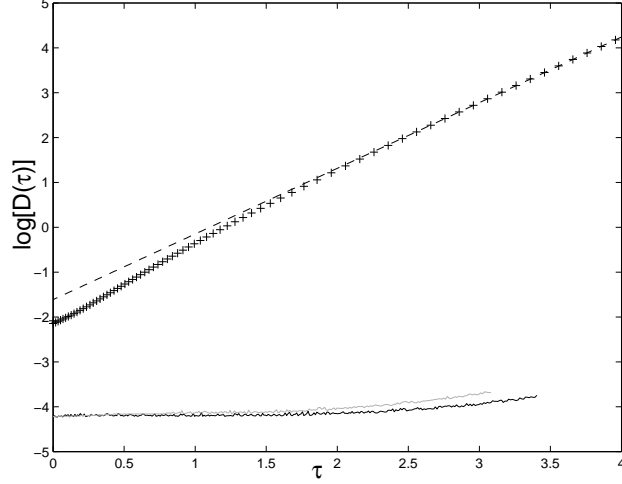


Figure 6:  $\tau$  evolution of the logarithm of the minimum distance between rescaled contours. Crosses stand for non collapsing initial data. The dashed linear fitting of the last  $N$  data provides a gradient  $m = 1.4742$  which confirms a non collapsing condition according to the limit (17). The black and gray solid lines respectively correspond to the evolution of the collapsing initial data of Fig 8a) and 8b).

initial data. The minimum distance,  $D(\tau)$ , between these patches evolves with  $\tau$  as indicated by crosses in Fig. 6. The logarithmic scale on the vertical axis confirms that the  $\tau$  evolution is in close correspondence to Eq. (13). A linear regression adjusting  $N = 16$  data in the interval  $\tau \in [1.5, 5.5]$  provides a gradient  $m = 1.4742$  very close to the limit of the collapse condition  $\delta = 1/\alpha = 1.4286$  provided in (17). In particular non collapse is guaranteed if  $m > \delta$ . Similar results would have been expected for any arbitrary rotation of the initial patches.

Simulations reported in [2] address the existence of collapsing initial data. In particular there it is reported that two circles in which  $\theta_k = -1$ , with unit radius and with centres placed at a distance 2.5, collapse in a finite time. The collapse is point-like and the symmetry of the initial data reports two collapsing points on each curve. Blow up also exists for initial data different from that discussed in [2]. For instance if the above described circles are deformed to two ellipses with semi-axis  $a = 1.1$  on the horizontal line and  $b = 1$  in the vertical line, the collapse regime described in [2] is also reached. The collapse time of these ellipses is estimated by means of a nonlinear adjustment as explained in [2, 19] and it is obtained that in this case  $t_* = 6.887794662$ . This value is used to rescale profiles according to expression (6). In particular we perform simulations in the self-similar variables taking as initial data the curves of this simulation

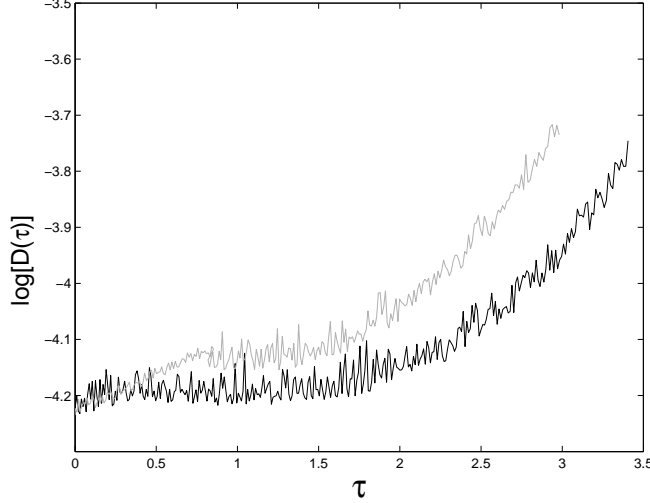


Figure 7:  $\tau$  evolution of the logarithm of the minimum distance between rescaled collapsing contours. The black line correspond to a simulation with low resolution  $\nu = 0.05$  and the gray line corresponds to the same initial data with a higher resolution  $\nu = 0.03$ . Both resolutions confirm a highly oscillating system.

at time  $t_{max} = 6.81482306$ , and rescaling them with the transformation (6). In this expression  $\vec{y}_* = (0, 0)$  and  $\vec{x}_*(t)$  is an unknown rescaling function. Figure 8 shows the two choices taken for it. In figure 8a) it is considered  $\vec{x}_*(t_{max}) = (0, 0)$  and in figure 8b) it is considered  $\vec{x}_*(t_{max}) = (1.36439899, -0.28345455)$  that moves the two collapse corners to the left (L). In Fig. 8a) the configuration is as follows: one patch overlaps regions (L), (U) and (R) while the other overlaps regions (L), (D) and (R). For the Fig. 8b) the configuration is: one patch is contained in region (L), while the other overlaps regions (L), (D) and (R). In both cases the minimum distance between patches evolves according to the collapse condition (17). The function  $\log(D(\tau))$  is depicted in Fig 6. The solid black line stands for the initial data of figure 8a) while the solid gray line corresponds to the initial data in figure 8b). Both regimes stay below the line which mark the limit for non collapsing initial data. Simulation are performed for a  $\tau$  interval in which the area of the patches increases 4 orders of magnitude.

Figure 7 shows a magnification of the evolution of  $\log(D(\tau))$  for the initial data in Fig. 8a). It is clear the rapidly oscillating behaviour that does not settle in a stationary regime as would be the case of an attracting fixed point. The black line corresponds to the evolution of the minimum distance with resolution  $\nu = 0.05$ , the gray line corresponds to a higher resolution ( $\nu = 0.03$ ). In the latter case the amplitude of the oscillations diminishes, but still confirms a “chaotic” evolution of the distance. It seems that these oscillations are under-resolved in both discretisations, and there is a noticeable sensitivity in



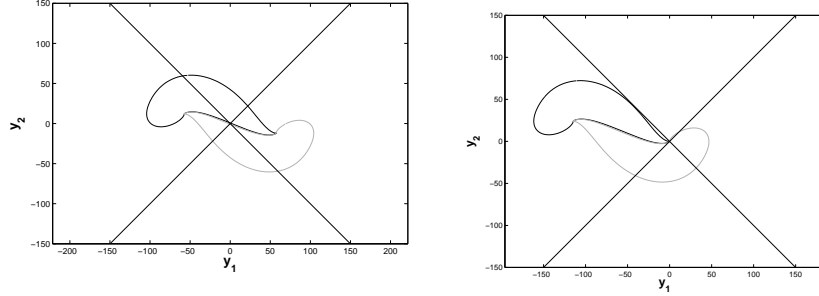


Figure 8: a) Initial collapsing data; b) A second initial collapsing data.

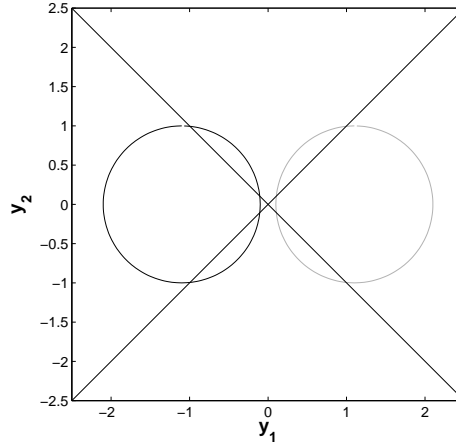


Figure 9: Initial data which collapse slowly.

the evolution to the dimension of the discrete system (25) which is different in both cases. This confirms the conjecture of a “chaotic” evolution embedded in an infinity dimensional dynamical system.

Fig. 9 shows another collapsing data distributed like in Fig. 8a). However in this case the non collapse configuration discussed in Fig. 5 (*i.e.* each patch is entirely contained in opposite domains) is only slightly violated. Numerically is found that the evolution of the distance between contours follows an exponential law as the initial data of Fig. 5 did. However now the gradient obtained from the linear fitting  $\tau$  vs  $\log(D(\tau))$  is  $m = 1.4187$ . This is almost equal to  $\delta$ , however it does not satisfy the non collapse requirement  $m > \delta$ , and thus the initial condition provides an example of a slowly collapsing data.

## 5 Conclusions

We have studied the  $\alpha$ -patches problem in self-similar variables and we have found a family of exact self-similar fixed points for these equations. These are valid for the whole parameter range  $0 < \alpha \leq 1$  which encompasses the surface quasi-geostrophic equation. For the  $\alpha = 0.7$  case intensive numerical simulations are performed. They indicate that the stationary solution organises the evolution of different initial data, since it acts as a separatrix of collapsing and non collapsing conditions. It is found a perturbation to this solution that completely fall in its unstable subspace. These are repelling patches that separate exponentially at a rate  $m > \delta$  thus confirming the non collapse requirement (17). The  $\tau$  evolution of other initial conditions is also discussed. There are found collapsing solutions for initial configurations that cross the boundaries marked by the fixed point (33). It seems that some of these data do not reach a stationary regime but a “chaotic” one. Also initial conditions that slowly collapse are reported.

## Acknowledgements

I wish to thank A. Córdoba, D. Córdoba, J. Eggers, C. Fefferman, M. A. Fontelos and J.L Rodrigo for their useful comments and suggestions. DC initiated me on  $\alpha$ -patches and proposed me the problem discussed in this article. JE, CF and MAF provided me with valuable insights on the self-similar transformation. MAF helped me in the evaluation of the integrals in Eq. (26) by means of series expansions. The computational part of this work has been performed on supercomputers at the BSC and CESGA to which I acknowledge worthful support.

This work has been supported by Consolider I-MATH (C3-0104) and CSIC grants No. PI-200650I224 and OCEANTECH (No. PIF06-059).

## References

- [1] Constantin, P. “On the Euler equation of incompressible fluids.” Bulletin of the American Mathematical Society **44** (2007), 4, 603-621.
- [2] Córdoba D., Fontelos M. A., Mancho A. M., Rodrigo J. L. “Evidence of singularities for a family of contour dynamics equations.” Proc. Natl. Acad. Sci. **102** (2005), 17, 5949-5952.
- [3] Bertozzi, A. L. and Constantin, P. “Global regularity for vortex patches”. Commun. Math. Phys. **152** (1993), no.1, 19-28.
- [4] Buttkke, T.F. “The observation of singularities in the boundary of patches of constant vorticity” Phys. Fluids A **1** (1989), 1283-1285.

- [5] Chemin, J. Y. “Persistence de structures géométriques dans les fluides incompressibles bidimensionnels”. *Ann. Ec. Norm. Supér.* **26** (1993), no.4, 1-16.
- [6] Constantin P., Majda, A. and Tabak E. “Formation of strong fronts in the  $2 - D$  quasi-geostrophic thermal active scalar”. *Nonlinearity* **7** (1994), n0. 6, 1495-1533.
- [7] Córdoba D., Fefferman C. and Rodrigo J.L. “Almost sharp fronts for the surface quasi-geostrophic equations” *Proc. Natl. Acad. Sci.*, 101 (2004), 2687-2691.
- [8] Dritschel, D.G. and McIntyre, M.E. “Does contour dynamics go singular?” *Phys. Fluids A* **2**(5) (1990), 748-753.
- [9] Dritschel, D.G. “Contour dynamics and contour surgery: numerical algorithms for extended, high-resolution modelling of vortex dynamics in two-dimensional, inviscid, incompressible flows” *Computer Physics Reports* **10** (1989), 77-146.
- [10] Hamilton, R. “The inverse function theorem of Nash and Moser”. *Bull. Amer. Math. Soc. (N.S.)* **7** (1982), no. 1, 65-222.
- [11] Majda A. and Bertozzi, A. “Vorticity and incompressible flow”. *Cambridge Texts in applied Mathematics*, 27 (2002).
- [12] Pedlosky, J. “Geophysical Fluid Dynamics”. Springer-Verlag, New York (1987), 345-368 and 653-670.
- [13] Rodrigo, J.L. “On the evolution of sharp fronts for the Quasi-geostrophic equation”. *Comm. Pure Appl. Math.* (2005), 58 (6) 821-866.
- [14] Zabusky, N., Hughes, M.H. and Roberts, K.V. “Contour dynamics for the Euler equations in two dimensions.” *J. Comp. Phys.* (1979), 96-106.
- [15] J. Eggers, M. A. Fontelos, “The role of selfsimilarity in singularities of PDE’s” , *Nonlinearity* 22 (1) (2009) R1-R44.
- [16] Pumir, A., Siggia E. D. “Development of singular solutions to the axisymmetric Euler equations” *Phys. Fluids A*, 4:1472, 1992.
- [17] W.H. Press, S.A. Teukolsky, W.T. Vetterling, B.P. Flannery, *Numerical Recipes in Fortran 77, The Art of Scientific Computing*, 2nd ed., Cambridge University Press, Cambridge, 1999.
- [18] F. Gancedo. “Existence for the  $\alpha$ -patch model and the QG sharp front in Sobolev spaces”. *Advances in Mathematics*, 217, (6), (2008), 2569-2598.
- [19] Jiménez, S.; Martín, I.M.; Mancho, A.M.; Pérez-García, V.M.; Vázquez, L. A “Conservative Numerical Scheme for the simulation of Blow-up in the Nonlinear Schrödinger equation”. *Appl. Math. Comput.* 134 (2003), 271-291.

- [20] Ponce Dawson, S. ; Mancho, A. M. “Collections of Heteroclinic Cycles in the Kuramoto-Sivashinsky Equation”. *Physica D* 100 (1997), 231-256.